DESIGN OF ARGON RUNNER IN POLYCRYSTALLINE SILICON DIRECTIONAL SOLIDIFICATION SYSTEM

Kai-Chun Lin, Yu-Yi Lin and Chao-Ming Hsu*

Department of Mechanical Engineering
National Kaohsiung University of Applied Sciences
No. 415, Chien Kung Rd., Sanmin Dist., Kaohsiung City 80778, Taiwan
*Corresponding author: jammy@kuas.edu.tw

Abstract. *In this paper, a new design and a better method for analyzing the opening angle of argon flow are proposed by numerical software (ANSYS). Simulate the growth process of long crystal furnace and establish a global 2D numerical model. Set the simulation rules to include argon flow and heating time and refer to the actual process. The model considers the heat transfer model, the flow field model and the thermal radiation factor, and changes the opening angle of the argon inlet runner to 20°, 60° and 140° during the simulation. The results indicate the following. When the opening angle of the argon flow path is 20°, a higher axial temperature difference is generated, so that the growth of the ingot can be accelerated. If a prototype furnace is used at the beginning of the crystal growth, a lower radial temperature difference occurs at a mid-60° and a later stage of 60°, which avoids the growth of the crystal grains on the side wall of the crucible.*
Keywords: Polycrystalline silicon, Directional solidification, Finite volume method

1. **Introduction.** The development of solar energy can date from 1839, when a French physicist, Physicist Becquerel found in the laboratory that there would generate current when the light is irradiated into the conductive liquid [1,2], and this is the Photovoltaic Effect. In 1883, an American scientist, Fritts made the first solar cell by coating a thin layer of gold on selenium (Se, a kind of semiconductor material), lifting the curtain on the development history of solar cells, but the energy conversion efficiency then was very low, only less than 1% [3]. Until 1946, Russel, a semiconductor research scholar, observed silicon (Si) also has the photovoltaic effect [4] and applied for the patent as the first person to make the modern solar cell, and then silicon was widely used for the solar energy technology. In 1954, the research scholars in Bell Labs, Chapin et al. found silicon's sensitiveness to light would be more intense after mixing some dopant in it; this experiment enabled the Bell Labs to make the first solar cell with application value and its photoelectric conversion efficiency was 6% [5,6]. Meanwhile, Rappapport research team of RCA Inc found the photovoltaic effect of cadmium (Cd) [7]. At present, though many scholars are researching the curing process of polycrystalline silicon ingot with the hope to produce high-quality solar cells, they still cannot change the fact that the photoelectric conversion efficiency of polycrystalline silicon chip is lower than that of monocrystalline silicon chip; just as the preparation process of polycrystalline silicon is simple and its manufacturing cost is lower, the mainstream product in the market currently is polycrystalline silicon solar cell [8,9]. The method of numerical analysis is improved with the improvement of computer equipment. More and more problems can be calculated by numerical analysis. In 2013, a mathematical model of the removal of impurities in molten silicon by electron beam melting was established. The results show that the reduction of the laser radius and the increase in the laser power rate will reduce the energy consumption [10]. In 2015, a two-dimensional global heat transfer mathematical model was established to simulate the

thermal behavior and thermal stress of long anchors [11]. In 2016, the crystal growth of polycrystalline silicon (mc-Si) was analyzed by numerical analysis in the directional solidification process. The simulation results show that the number of silicon grains decreases with increasing crystal length [12].

2. **Research Method.** In the process of crystal growth, the argon used is to cool the silicon liquid and the silicon ingot will be cured into ingot from liquid after cooling. At the other hand, the flow or turbulent flow of argon can indirectly take the surface impurity of the silicon liquid away, so argon plays an important role in the growth process of silicon ingot; the flow amount and the turbulent flow shape of argon passing the silicon liquid are also the key factors influencing the performance of the solar cells. The temperature during the growth process will reduce slowly, and the insulation cage can be lifted gradually according to the setting of preparation process, in order to get a higher cooling rate for the crucible bottom and enable the silicon crystal particles to grow upward from the bottom. When the silicon ingot solidifies completely, there will be a given obvious temperature gradient on the silicon ingot from the bottom to the top, this temperature gradient can generate thermal stress or tiny stress crack in the silicon ingot, under this situation, if the silicon ingot is directly cooled to the room temperature, it will crack caused by the overlarge thermal stress in it, resulting in loss of yield rate; therefore, it needs to anneal for a while and eliminate the thermal stress in the silicon ingot. The cooling process begins after the heater is shut down, and the silicon ingot will be cooled to the room temperature by using large quantity of argon, facilitating the subsequent processing. This research will simulate and analyze the growth process and discuss the growth direction of silicon ingot and the change of temperature field.

This research is mainly to simulate and analyze the thermal field of the preparation process for crystal growth directing at the DSS450 crystal growth furnace developed by GT-Solar, an American company. The analysis model is a 2D Global Model constructed with AutoCad, as shown in Figure 1. The inner parts of the DSS crystal growth furnace used for this research are diverse and in complex shapes, and the total number of elements is up to 3,500,000 after constructing the 3D geometric model and dividing the mesh number, so it is very difficult to control the model quality within an ideal scope, this will result in too long time for object analysis and accuracy deviation after analysis, so the 2D geometric model is adopted for value analysis, to reduce the total number of meshes,
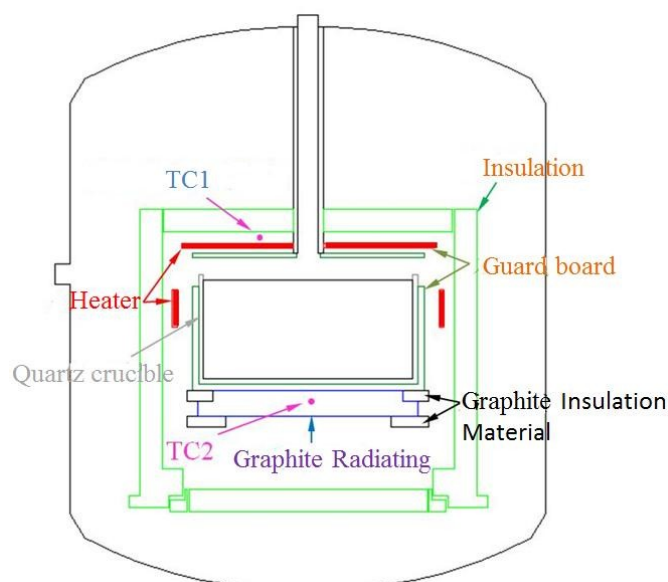

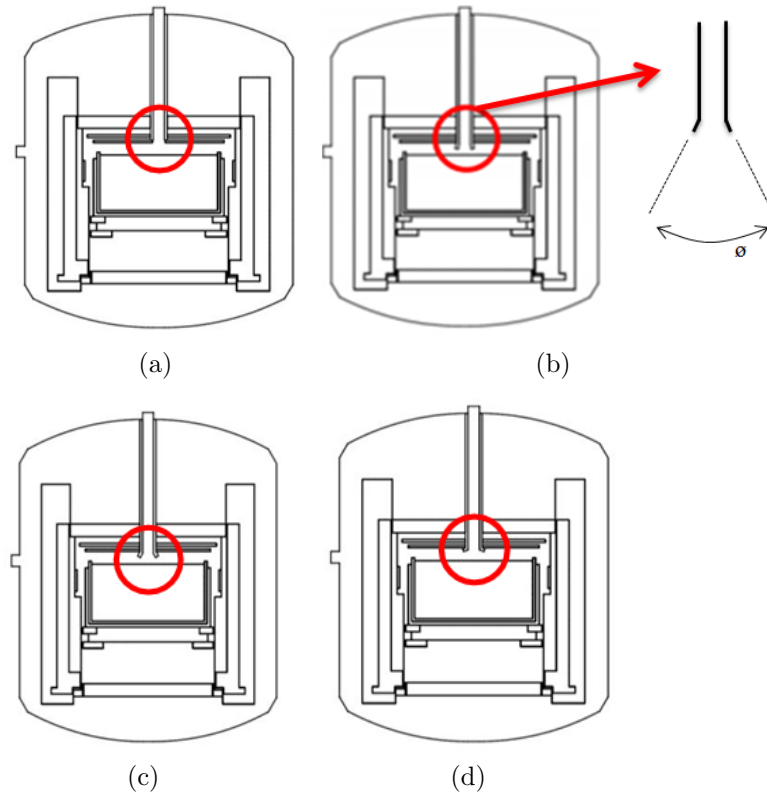FIGURE 1. Model of polycrystalline silicon crystal growth furnace

FIGURE 2. Designed opening angle of argon runner: (a) prototype furnace; (b) $\phi = 20°$; (c) $\phi = 60°$; (d) $\phi = 140°$

enhance the mesh quality and significantly reduce the time for value calculation. Figure 2 shows 2D model of the prototype furnace and designed opening angle of the argon runner; the angles are 20°, 60° and 140°. The insulation cage meshes can be divided into movable area and immovable area; triangular unstructured meshes are used around the immovable area, to realize automatic remeshing of partial areas during calculation.

3. Result and Discussion.

3.1. **Simulation result of prototype polycrystalline silicon crystal growth furnace.** The slope is defined to discuss the shape changes of the solid-liquid interface during the curing process of ingot [13], there will be a minimum position in the solid-liquid interface, the area from this minimum position to the side wall of the crucible is called wall area, the maximum position of the wall area is generally on the wall of the crucible, and the average slope of the solid-liquid interface in the wall area worked out with the maximum and minimum positions is called concavity; the area from the minimum position to the center of the crucible is called central section, the maximum position of the solid-liquid interface in the central section is generally at the center of the silicon liquid, and the average slope of the solid-liquid interface in the central section worked out with the maximum and minimum positions is called convexity. The concavity is defined as a negative value and the smaller the value is, the more concave the shape of the solid-liquid interface in the wall area; the convexity is defined as a positive value, the larger the value is, the more convex the shape of the solid-liquid interface in the central section. The mathematical expressions of the concavity and convexity are as follows:

$$\text{Concavity} = -\frac{dy_2}{dx_2} \qquad (1)$$

$$\text{Convexity} = -\frac{dy_1}{dx_1} \qquad (2)$$

There are 6 expected lifting positions set in the silicon liquid and the temperature changes of each position when the crystal growth process are observed. Three positions of them are marked as A, B and C and they are respectively 30mm, 200mm and 370mm away from the bottom of the silicon liquid. The other three positions are marked as A*, B* and C* and they are respectively located at the left side of A, B and C with a distance of 390mm (the distance to the wall surface of the crucible is 30mm), and their relative positions are shown in Figure 3.

Figure 4 and Figure 5 are the time-temperature curves charts of the simulation process for the positions for silicon liquid; there are 6 line segments, the vertical interval between them is the temperature difference between two points; if the interval is larger, it indicates the axial temperature gradient is larger and the possibility of the crystal particles' vertical and upward growth is higher. In the 5-hour curing process, as the position A in the silicon liquid firstly solidifies into solid silicon, while position C is still liquid silicon with the temperature higher than 1685K at this moment; because the heat transfer feature of solid silicon is better than that of liquid silicon and the silicon at the bottom cools more quickly, the temperature difference between two positions before the solidification of position C will increase gradually and the maximum temperature difference is 39.41K; the temperature difference will decrease gradually after position C solidifies at the 36th hour or so. In order to determine the minimum position needed by the concavity and convexity, the position of 50% of the solid-liquid fuzzy region is defined as the solid-liquid interface. The inner and outer wall surfaces on both sides of the crucible cool faster, which causes the crystal
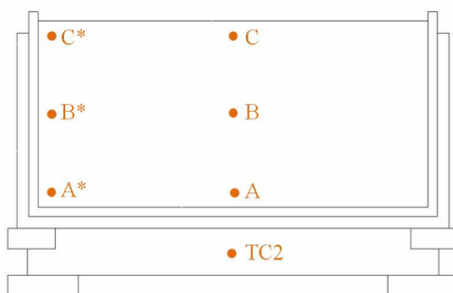

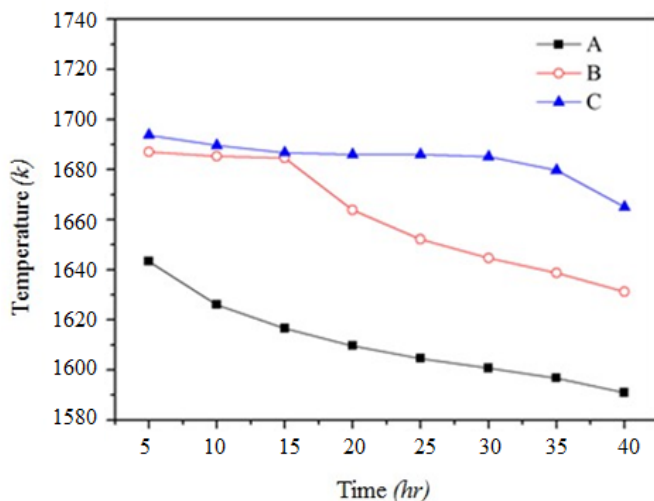FIGURE 3. Positions for silicon liquid

FIGURE 4. Curve chart of the temperature field at position A, B and C in the prototype furnace
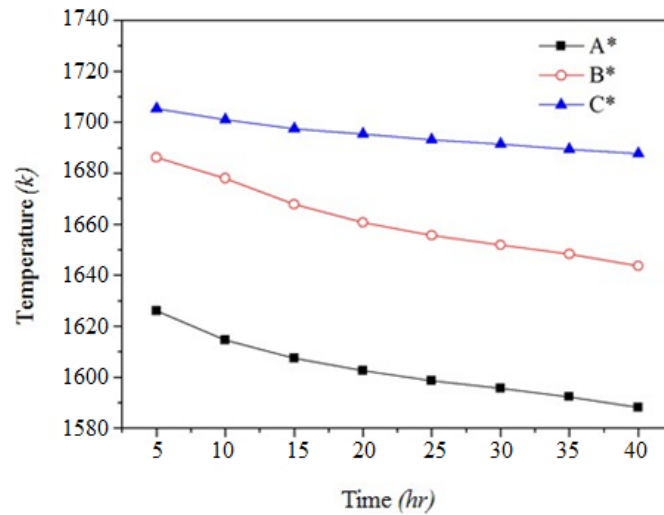
FIGURE 5. Curve chart of the temperature field at position A*, B* and C* in the prototype furnace

meshes grow inward from the wall surface, so if the radial temperature gradient can be controlled to be not too large in the preparation process, the crystal particles' growing from the crucible wall firstly can be avoided; the crystal particles growing inward from the crucible wall will make the crystal meshes in the silicon chip present the long-striped shape and form the defect of dislocated meshes; too large meshes can cause the impurity in the silicon gets together at the crystal interface and too high impurity concentration can seriously affect the photoelectric conversion efficiency of the silicon chip.

3.2. **Simulation result of the crystal growth furnace with the designed argon runner angle.** Figure 6 is the curve chart of the temperature difference between position A and B when the argon inlet in the furnace is changed into 20°. The maximum temperature difference between position A and B is 36.35K, 3.06K lower than that of the prototype furnace. It can be seen from the figure about 30 hours after curing. Figure 7 is the radial temperature change curve, the radial temperature difference is the radial temperature difference between the central position and the position on the wall surface, and low radial temperature difference can avoid the crystal particles' growing firstly from the crucible wall. Position C solidifies firstly at the 36th hour as being affected more
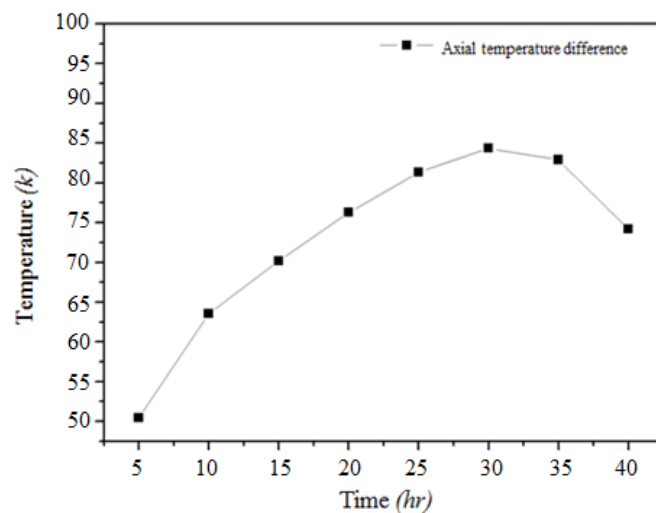

FIGURE 6. Axial temperature difference when the opening angle of the argon runner is 20°
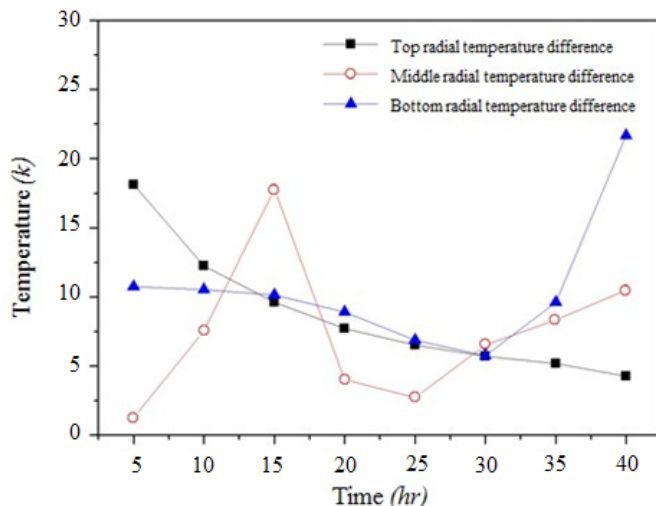
FIGURE 7. Radial temperature difference when the opening angle of the argon runner is 20°
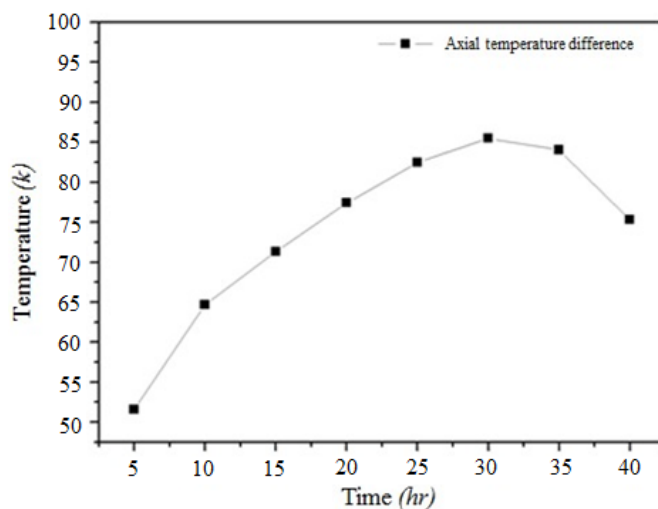

FIGURE 8. Axial temperature difference when the opening angle of the argon runner is 60°

seriously by the gathering of argon flow, while the temperature at position C* is kept at 1685K because it is nearer to the heater; therefore, the temperature difference is gradually increasing. Position B* solidifies firstly at the 5th hour, position B solidifies after the 16th hour, the maximum temperature difference between these two positions is 16.53K which is 0.48K higher than that of the prototype furnace; when position B solidifies, radial temperature difference will fall off. Position A* solidifies instantly at the early period of growth, position A solidifies at the 0.6th hour, the radial temperature difference at this position gradually falls off and the maximum temperature difference between these two positions at the 5th hour is 10.73K, 1.96K higher than that of the prototype furnace.

When the runner opening angle is 60°, the argon inlet in the crystal growth furnace is changed into 60°. Figure 8 is the curve of the temperature difference between position A and C. During the curing process at the 5th hour with the argon runner opening angle of 60°, the maximum temperature difference between position A and C is 37.3K, 2.1K lower than that of the prototype furnace. Figure 9 is the radial temperature change curve during the curing process. Position C solidifies firstly at the 36th hour as being affected more seriously by the gathering of argon flow, while the temperature at position C* is kept at 1685K because it is nearer to the heater; therefore, the temperature difference is
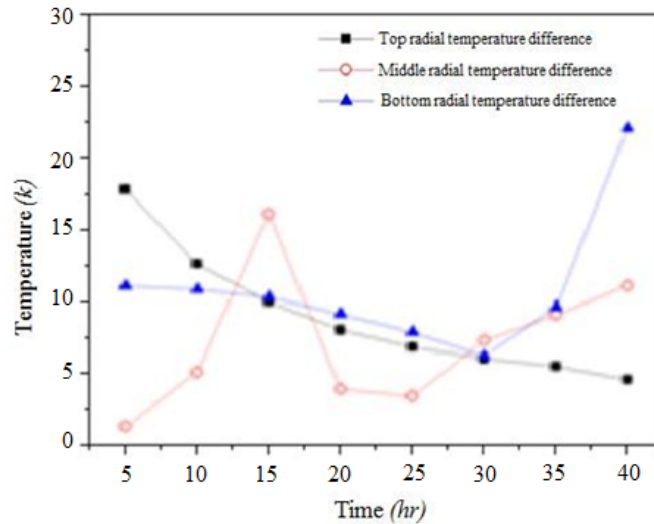
FIGURE 9. Radial temperature difference when the opening angle of the argon runner is 60°
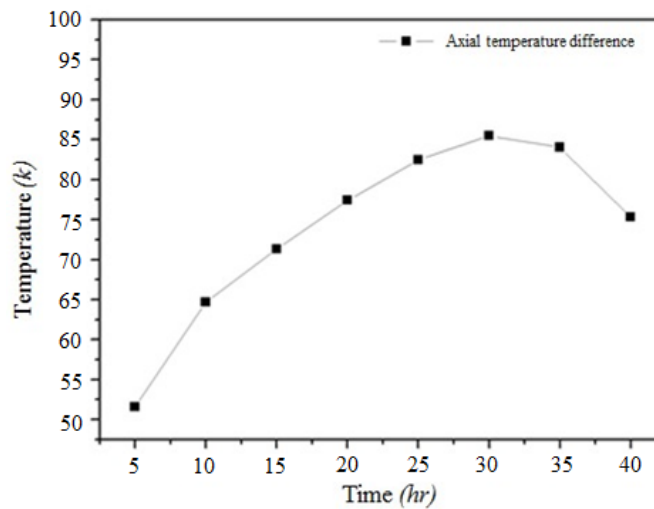

FIGURE 10. Axial temperature difference when the opening angle of the argon runner is 140°

gradually increasing. Position B* solidifies firstly at the 5th hour, position B solidifies after the 16th hour, and the maximum temperature difference between these two positions is 14.62K, 1.42K higher than that of the prototype furnace; when position B solidifies, radial temperature difference will fall off. Position A* solidifies instantly at the early period of growth, position A solidifies at the 0.6th hour, the radial temperature difference at this position gradually falls off and the maximum temperature difference between these two positions at the 5th hour is 10.73K, 1.96K higher than that of the prototype furnace.

When the argon runner opening angle is 140°, the argon inlet in the crystal growth furnace is changed into 140°, which is the largest opening angle for the inlet. Figure 10 is the curve of the temperature difference between position A and C, representing the axial temperature changes. During the curing process at the 5th hour with the argon runner opening angle of 140°, the maximum temperature difference between position A and C is 39.96K, 0.55K higher than that of the prototype furnace. Figure 11 is the radial temperature change curve during the curing process. Position C solidifies firstly at the 36th hour as being affected more seriously by the gathering of argon flow, while the temperature at position C* is kept at 1685K because it is nearer to the heater; therefore, the temperature difference is gradually increasing. Position B* solidifies firstly at the 5th
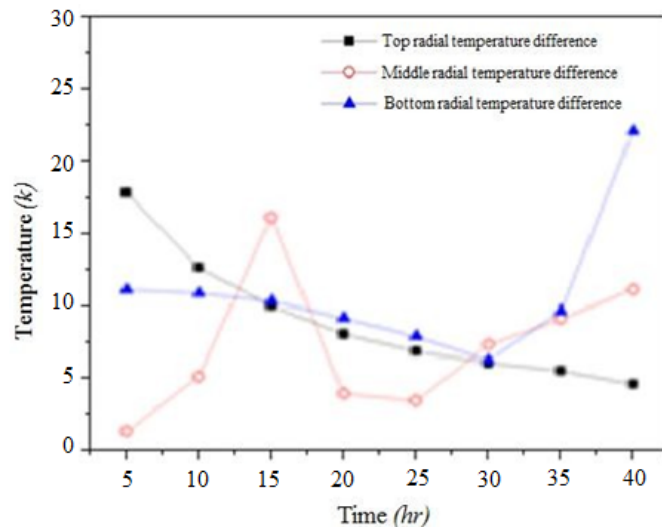
FIGURE 11. Radial temperature difference when the opening angle of the argon runner is 140°

hour, position B solidifies after the 16th hour, and the maximum temperature difference between these two positions is 14.72K, 1.33K lower than that of the prototype furnace.

4. **Conclusions.** This research mainly discusses the influences of the designed argon inlet opening runner on the temperature field and solid-liquid interface during the crystal growth process.

1. The axial temperature difference is higher when the angle is 20°, which can expedite the growth of the ingot and reduce the cost of preparation process.

2. The smaller argon runner opening during the early growing period of polycrystalline silicon ingot is favorable for the formation of the convex solid-liquid interface, which can make the impurities in the polycrystalline silicon ingot be pushed to all around and enlarge the argon runner opening after the metaphase (15 hours), being favorable for the overall growth of the ingot, reducing the time of preparation process and saving the cost.

3. During the crystal growth metaphase (10-20 hours), the argon opening angle can be 20°, 60° and 140°, to obtain lower middle radial temperature difference; 60° is the best.

4. More and more studies use numerical analysis to simulate the process of long crystal. Many related studies have shown a complete heat transfer model. And then use the global two-dimensional numerical model to propose new designs in the future.

REFERENCES

[1] A. E. Becquerel, Mémoire sur les effets électriques produits sous l'influence des rayons solaires, *Comptes Rendus de l'Académie des Sciences*, vol.9, pp.561-567, 1839.
[2] R. Williams, Becquerel photovoltaic effect in binary compounds, *The Journal of Chemical Physics*, vol.32, pp.1505-1514, 1960.
[3] C. E. Fritts, On a new form of selenium cell, and some electrical discoveries made by its use, *American Journal of Science*, vol.26, pp.465-472, 1883.
[4] *Light Sensitive Device*, U.S. Patent: 2,402,662, 1946.
[5] D. M. Chapin, C. S. Fuller and G. L. Pearson, A new silicon p-n junction photocell for converting solar radiation into electrical power, *Journal of Applied Physics*, vol.25, no.5, pp.676-677, 1954.
[6] J. Perlin, *Silicon Solar Cell Turns 50*, National Renewable Energy Laboratory, Golden, CO. (US), 2010.
[7] D. A. Jenny, J. J. Loferski and P. Rappaport, Photovoltaic effect in GaAs p-n junctions and solar energy conversion, *Physical Review*, vol.101, no.3, pp.1208-1209, 1956.
[8] D. Sarti and R. Einhaus, Silicon feedstock for the multi-crystalline photovoltaic industry, *Solar Energy Materials and Solar Cells*, vol.72, nos.1-4, pp.27-40, 2002.

[9] G. Muller and J. Friedrich, Optimization and modeling of photovoltaic silicon crystallization processes, *Selected Topics on Crystal Growth*, vol.1270, pp.255-281, 2010.

[10] Y. Tan, S. Wen, S. Shi, D. Jiang, W. Dong and X. Guo, Numerical simulation for parameter optimization of silicon purification by electron beam melting, *Science Direct*, vol.95, pp.18-24, 2013.

[11] L. Liu, Q. Yu, X. Qi, W. Zhao and G. Zhong, Controlling solidification front shape and thermal stress in growing quasi-single-crystal silicon ingots: Process design for seeded directional solidification, *Science Direct*, vol.91, pp.225-233, 2015.

[12] Q. Lian, W. Liu, R. Li, W. Yan, C. Liu, Y. Zhang, L. Wang and H. Chen, Numerical simulation of multi-crystalline silicon crystal growth using a macro-micro coupled method during the directional solidification process, *Applied Sciences*, vol.7, no.1, 2017.

[13] Y.-Y. Teng, J.-C. Chen, C.-W. Lu and C.-Y. Chen, The carbon distribution in multicrystalline silicon ingots grown using the directional solidification process, *Journal of Crystal Growth*, vol.312, pp.1282-1290, 2010.